frontiers | Frontiers in Marine Science

TYPE Original Research
PUBLISHED 08 May 2025
DOI 10.3389/fmars.2025.1535411

OPEN ACCESS

EDITED BY
Sergio Maldonado,
Tecnologico de Monterrey, Mexico

REVIEWED BY
Guoxiang Wu,
Ocean University of China, China
Debin Sun,
Chinese Academy of Sciences (CAS), China

*CORRESPONDENCE
Fanzhu Qu
fanzhuqu@163.com
Ling Meng
lmeng@yic.ac.cn

RECEIVED 27 November 2024
ACCEPTED 14 April 2025
PUBLISHED 08 May 2025

CITATION
Wang F, Bi X, Qu F, Zou T, Wang XH and Meng L (2025) Interannual dynamics of the Yellow River turbid plume: the role of the water–sediment regulation scheme. *Front. Mar. Sci.* 12:1535411. doi: 10.3389/fmars.2025.1535411

Interannual dynamics of the Yellow River turbid plume: the role of the water–sediment regulation scheme

Fujia Wang[1], Xiaoli Bi[2], Fanzhu Qu[1]*, Tao Zou[2], Xiao Hua Wang[3] and Ling Meng[2,3]*

[1]The Institute for Advanced Study of Coastal Ecology, Ludong University, Yantai, China, [2]CAS Key Laboratory of Coastal Environmental Processes and Ecological Remediation, Yantai Institute of Coastal Zone Research, Chinese Academy of Sciences, Yantai, China, [3]The Sino-Australian Research Centre for Coastal Management, University of New South Wales Canberra, Canberra, ACT, Australia

The water–sediment regulation scheme (WSRS), initiated in 2002, induced an impulse delivery of freshwater and sediment within 10–20 days. In this scenario, the Yellow River turbid plumes (YRPs), which serve as indicators of the marine dispersion of terrestrial materials, displayed substantial spatio-temporal variations. However, the extension patterns of the YRP and their dynamic mechanisms on an interannual scale remain poorly understood. Using multi-source high-resolution imageries, the YRP variations were examined during 2003–2023. The results revealed that the WSRS significantly increased the extensions of the YRP, with its area expanding annually from 67.41 ± 25.27 to 162.54 ± 39.03 km^2. Additionally, three distinct diffusion patterns were identified: I) a frequent prototypical spreading along the direction of river channel expansion, II) rightward spreading toward Laizhou Bay, and III) leftward spreading toward Bohai Bay. River discharge was identified as the primary driver controlling the plume extension, followed by wind, which primarily modulated the plume orientations. Furthermore, several unique plume extension patterns were observed under episodic weather events.

KEYWORDS

river plume, water discharge, wind forcing, water-sediment regulation scheme, Yellow River

1 Introduction

Large rivers serve as the main channels of material transport to the sea, which play an indispensable role as carriers in the global hydrological cycle (Chu et al., 2006; Wang et al., 2010a). When low-salinity freshwater from estuaries flows into high-salinity seawater, river plumes are generated, transporting large fluxes of dissolved nutrients and particulate matter to continental shelf seas, thereby influencing coastal biogeochemical and water quality (Warrick and Farnsworth, 2017). Spatio-temporal variations in plume size, shape,

and direction are largely influenced by river discharge, suspended sediment, wind forcing, estuary morphology, tidal forces, coastal current, and the Coriolis force (Yu et al., 2013a; Horner-Devine et al., 2015; Wu et al., 2023). Among these factors, river discharge and wind are widely recognized as the most important forcing mechanisms (Machaieie et al., 2022).

The Yellow River has relatively low water discharge but a high sediment load, making it a distinctive river in the global river system (Peng et al., 2010; Zhao et al., 2023). Since 2002, to address the issue of riverbed elevation caused by excessive sediment accumulation, the Yellow River Conservancy Commission has implemented the water–sediment regulation scheme (WSRS) at the beginning of each flood season (generally in mid-June to early July). During the WSRS, a substantial amount of water and sediment from reservoirs and the riverbed is transported to the Yellow River estuary (YRE) through this pulse delivery, significantly altering the seasonal patterns of water discharge and sediment load (Wang et al., 2010a). The WSRS currently accounts for 14%–55% of the annual water discharge and 26%–66% of the annual sediment load (Li et al., 2017; Wang et al., 2017c). This pulsed delivery of water and sediment provides an ideal case for studies on spatio-temporal variations in river plumes associated with human activities.

Many works have focused on the dispersal and related dynamics of the Yellow River turbid plume (YRP). Wang et al. (2008) demonstrated that the seasonal behavior of the YRP is primarily modulated by wind field variability, while tidal currents promote the offshore spread of low-salinity water and hinder alongshore downstream expansion of the plume. Bi et al. (2010) documented that the combined shear fronts and alongshore tidal currents were the major dynamic factors controlling the sediment dispersion near the present sub-delta. Cheng et al. (2021a) provided comprehensive evidence that wind forcing constitutes the primary driver of seasonal YRP variability while additionally elucidating how bathymetric evolution and river discharge regulate plume extension patterns. Focused on the WSRS event, the *in situ* measurements revealed that the plume pathway shifted rapidly resulting from intensive interactions between river discharge and the varying bathymetry in the river mouth area in response to the WSRS in 2005 (Wang et al., 2005). The intraday variation observed from geostationary Geostationary Ocean Color Imager (GOCI) data clearly illustrated the dominance of tidal current on short-term dispersal patterns of freshwater and sediment plumes (Guo et al., 2017). Both the hydrographic data and modeling results show that the Yellow River plume propagates upstream under the low river discharge condition in summer but turns downstream under the high river discharge condition (Yu et al., 2021). However, these extensive research efforts are limited by restricted data or focused on individual events or short time scales. To date, there has been no specific research about the influence of the WSRS on the interannual variation of the YRP.

Due to the aforementioned limitations, in this study, high-resolution imageries from 2003 to 2023 were involved to explore the dynamic variability of the YRP before and after the implementation of the WSRS. The main objectives are as follows: 1) to provide a synthetic view of the spatio-temporal variations of the YRP before and after the WSRS, 2) to reveal the interannual variability of the plume and classify its typical patterns, and 3) to investigate the responses of plume patterns to river discharge, wind forcing, estuary morphology, and coastal current.

2 Study area and materials

2.1 Study area

The Yellow River, originating from the Qinghai–Tibet Plateau and stretching from southwest to northeast, empties into the Bohai Sea in Kenli County of Dongying City (Figure 1) (Cai et al., 2023). With a total length of 5,464 km and a drainage area of approximately 7.95×10^5 km^2 (Yuan et al., 2024), the Yellow River discharged an annual average of 18.42×10^9 m^3 of water into the sea between 2008 and 2014 (Yan, 2019). The region has a warm temperate continental monsoon climate, characterized by

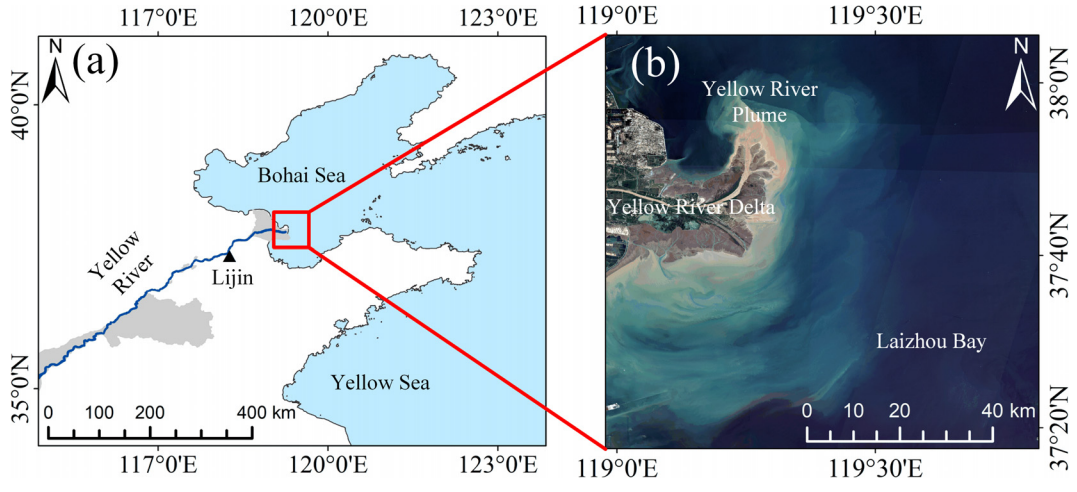

FIGURE 1
Location of the study area displaying the extent of the Yellow River Basin **(a)** and the YRE **(b)**. YRE, Yellow River estuary.

gentler waves in summer due to mild southerly winds (3–6 m/s) and intensified wave activity in winter driven by stronger northerly winds (>10 m/s) (Wang et al., 2014). In this area, the tides are irregular semidiurnal, with coastal currents with velocities between 0.5 and 1.0 m/s. These currents exhibit a reciprocating pattern, flowing southeastward during flood tides and northwestward during ebb tides (Li et al., 2023). Since the 1950s, extensive dam construction has taken place in the Yellow River watershed, with over 3,100 reservoirs collectively boasting a capacity exceeding 72×10^9 m^3. These reservoirs play a pivotal role in regulating water flow and mitigating sedimentation issues in the Yellow River basin (Lu et al., 2022). Although the expansion rate of the current Yellow River delta has gradually slowed down due to decreases in sediment discharges, the Yellow River delta still covers an area of 5,113 km^2 (Liu et al., 2020b). The main channel was artificially moved northward from the Qingshuigou waterway to Qingbacha in 1996, forming the current YRE between Bohai Bay and Laizhou Bay (Fu et al., 2021). Additionally, the estuarine distributary mouths have undergone notable shifts in recent years, exhibiting a distinct seaward extension (Li et al., 2023).

2.2 Data

High-resolution surface reflectance images, including Landsat 5 TM, Landsat 7 ETM+, and Landsat 8 OLI acquired from the Google Earth Engine (GEE; https://earthengine.google.com/), plus HJ-1A/B (Huanjing) CCD, HJ-2A/B CCD, and GF-1 (GaoFeng) WFV obtained from the China Centre for Resources Satellite Data and Application (CRESDA; https://data.cresda.cn/), were used to analyze the spreading dynamics of the YRP (Table 1). A total of 26 high-quality scenes (i.e., cloud cover <10%, low tide level) covering the YRE, acquired both before and after the implementation of the WSRS, were selected for this study.

TABLE 1 Information of high-resolution imagery (2003–2023).

Acquired date	Sensor type	Acquired date	Sensor type
2003-08-07	TM	2014-07-06	CCD
2003-09-24	TM	2015-05-20	OLI
2007-05-06	ETM+	2015-07-13	WFV
2007-07-17	TM	2019-05-31	OLI
2008-05-16	TM	2019-07-08	WFV
2008-07-03	TM	2020-06-02	OLI
2009-05-19	TM	2020-07-15	WFV
2009-07-06	TM	2021-05-04	OLI
2010-05-06	TM	2021-07-11	CCD
2010-09-11	CCD	2022-04-21	OLI
2011-06-02	ETM+	2022-07-08	CCD
2011-07-05	CCD	2023-06-05	OLI
2014-05-01	OLI	2023-07-14	CCD

Long time series of daily runoff and sediment load data recorded at the Lijin Hydrological Station (2003–2023), the closest station to the YRE, were collected to analyze variations in water discharge and sediment supply influenced by the WSRS. To assess the effects of wind forcing and ocean current effects on the river plume, hourly sea surface wind data at a 0.125° × 0.125° grid resolution from the fifth-generation European Centre for Medium-Range Weather Forecasts (ECMWF) atmospheric reanalysis dataset (ERA5) were utilized, along with 3-hourly ocean surface currents derived from the global 1/12° product of the Hybrid Coordinate Ocean Model (HYCOM) surface product. These datasets have demonstrated high accuracy in the Bohai Sea region (Lv et al., 2014; Wang et al., 2016).

2.3 Plume extraction and plume area calculation

The ocean color signal of river plumes, often characterized by high turbidity, is typically well correlated with surface salinity, which serves as a natural tracer of freshwater plumes (Binding and Bowers, 2003; Molleri et al., 2010; Mendes et al., 2017). Among the visible spectrum bands available in Landsat imagery, the Rrs645 band is more suitable for mapping the YRP due to its strong correlation with river discharge and its high sensitivity to river plume dynamics (Aurin et al., 2013; Fernández-Nóvoa et al., 2015; Guo et al., 2017; Maciel et al., 2021). Thus, a red band threshold approach was adopted in this study to detect the plume area, with a threshold value of 0.14 determined based on the findings of Chang et al. (2022). Through visual inspection, it is evident that our method effectively captures plume information (Figure 2).

The plume area was calculated by counting the number of pixels with Rrs645 equal to or above the threshold and multiplying by pixel size. The workflow structure is illustrated in Figure 3. The entire Landsat data processing was conducted using GEE, while the processing of CRESDA images was performed using ENVI 5.6.

3 Results

3.1 Water and sediment variations during WSRS

Figure 4 presents the daily average runoff and sediment load recorded at Lijin Hydrological Station since 2002. The data reveal that the WSRS was generally implemented from mid-June, with the exception of 2003, when it commenced on September 6 due to unusual autumn floods (Yu et al., 2013b). The duration of the WSRS varied significantly across years, ranging from a minimum of 7 days in 2014 to a maximum of 20 days in 2011 and 2019 (Figure 4c).

The first sudden increase in discharge was observed around June 25 at the Lijin Hydrological Station, occurring 4 or 5 days after

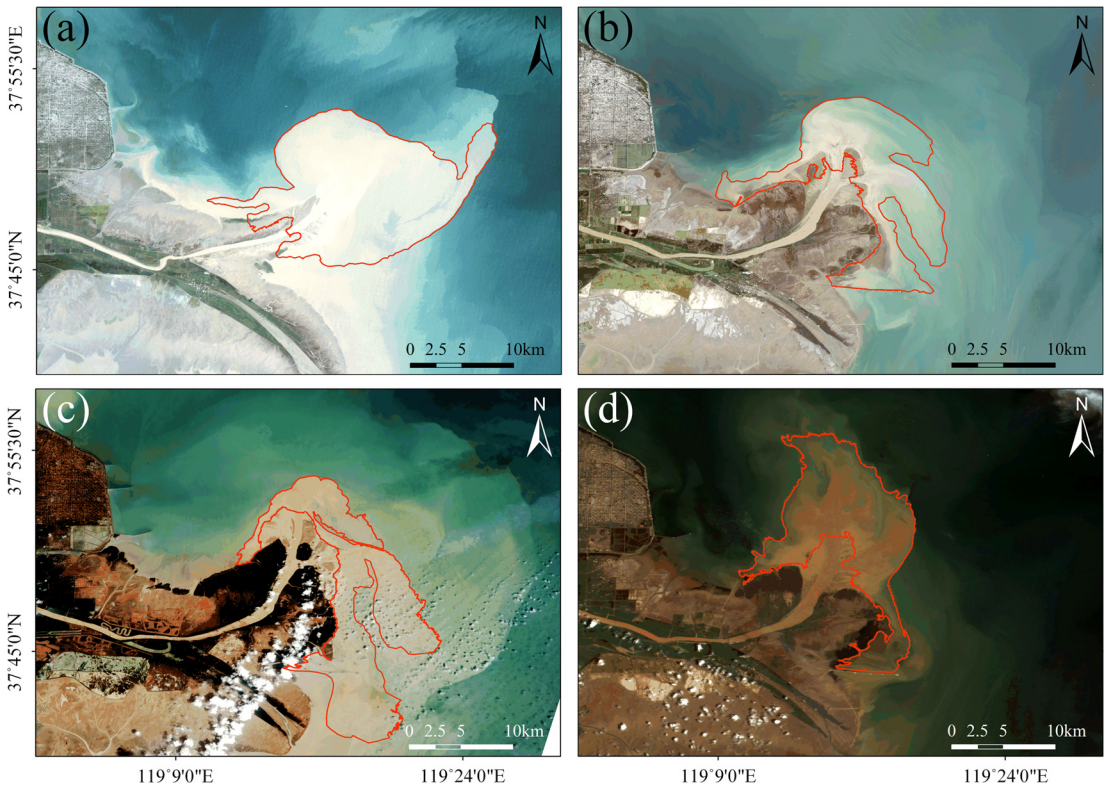

FIGURE 2
Plume extraction using different sensors based on red band threshold method; the red line range is the extracted YRP. **(a)** TM, **(b)** OLI, **(c)** WFV, and **(d)** CCD. YRP, Yellow River turbid plume.

the implementation of the WSRS. This decay is attributed to the distance of approximately 800 km between Lijin station and Xiaolangdi (Li et al., 2017). Subsequently, the discharge at Lijin station increased steadily from less than 800 to an average of 3,500 m^3/s, reaching its peak 10–15 days post-WSRS initiation. The high kinetic energy flow scoured the riverbed, leading to a significant increase in sediment concentration (Li et al., 2017). As a result, the sediment content at Lijin station rose sharply from 3 to approximately 20 kg/m^3, reaching its first peak within 4 to 6 days. Then, the export of fine-grained sediment from the Xiaolangdi Reservoir during the sediment regulation period contributed to the formation of the second sediment peak around mid-July (Wang et al., 2017b).

The maximum water discharge, maximum sediment content, total water discharge, and sediment load to the sea during the WSRS varied significantly from 2003 to 2023 (Figure 4c). These variations were primarily influenced by the volume of water stored in the Xiaolangdi Reservoir and upstream reservoirs prior to the WSRS (Wang et al., 2017a).

3.2 Spatio-temporal changes of YRP during WSRS

As shown in Figure 5, the spatial structure of the YRP exhibited significant interannual variability. Before the WSRS, the YRP occupied a relatively narrow stripe along the coastline, with its extension axis aligned with the estuary. The maximum seaward extension distance ranged from 3.70 to 16.36 km. After the WSRS, the plume morphology displayed considerable variation in horizontal scale, often characterized by a distinct fan-shaped diffusion extending 30° on either side of the river-to-sea extension line (Figure 5a) as the typical ideal, undisturbed pattern, similar to the prototypical large-scale plume described by Horner-Devine et al. (2015). Then, using it as a judgment criterion, the extracted plumes were further categorized based on the extent of lateral displacement of different plume areas. Based on the plume structure, after the WSRS, three major patterns of the YRP could be identified by satellite snapshots of turbidity images (Figure 5): 1) Pattern I, prototypical spreading along the direction of river channel expansion, such as the plumes observed in 2003, 2008, 2009, 2014, 2021, and 2022; 2) Pattern II, rightward spreading toward Laizhou Bay, observed in 2007, 2011, 2019, and 2020; and 3) Pattern III, leftward spreading toward the Bohai Bay, represented by 2010, 2015, and 2023.

Among the three patterns described above, Pattern I (46.15%) occurred most frequently, followed by Pattern II (30.77%), while Pattern III (23.08%) was observed to have the lowest occurrence frequency. Plumes classified as Pattern I mainly extend along the direction of river channel expansion. A stronger buoyant flow could broaden the seaward extension distance, particularly in years with a single estuary. In such cases, the plumes exhibit a significant northeastward extension, reaching up to 24.06 km, as far as 119° 25′E and 38°01′N. Pattern II plumes usually have a southeastward

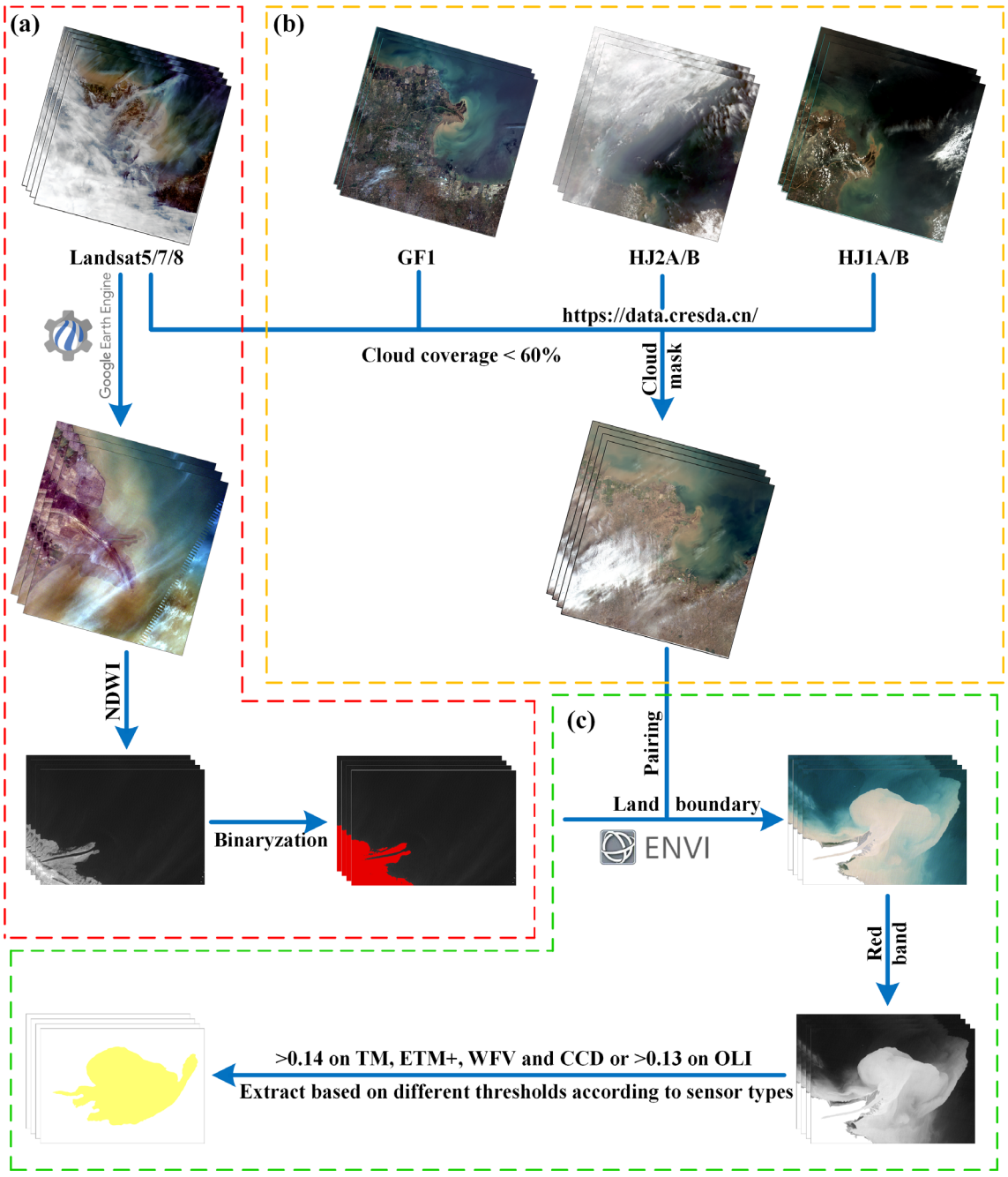

FIGURE 3
Flowchart of river plume extraction. **(a)** Data screening process; **(b)** Identification of land-sea boundaries; **(c)** Extraction of plume data.

tongue in the front, with the southern boundary of the plume extending as far as 37°40′N. In contrast, Pattern III plumes extend entirely northwestward, with most of the plume water moving toward nearshore, accompanied by limited offshore extension. However, year 2010 was an exception, with the northernmost tip reaching 37°58′N, approximately 16.36 km from the estuary.

The time series of YRP areas (Figure 6) revealed significant interannual variability in the plume both before and after the implementation of the WSRS. Before the WSRS, the average YRP value was 67.41 ± 25.27 km^2. The maximum area of the YRP could reach 117.47 km^2 in 2015, while the minimum area was only 18.27 km^2 in 2007. After the implementation of the WSRS, the plume area increased to 1.11–2.86 times its pre-WSRS size, with a sharp rise observed in 2010 when the area reached as high as 150.39 km^2. Notably, the plume area exhibits a slight interannual increasing trend both before and after the implementation of the WSRS.

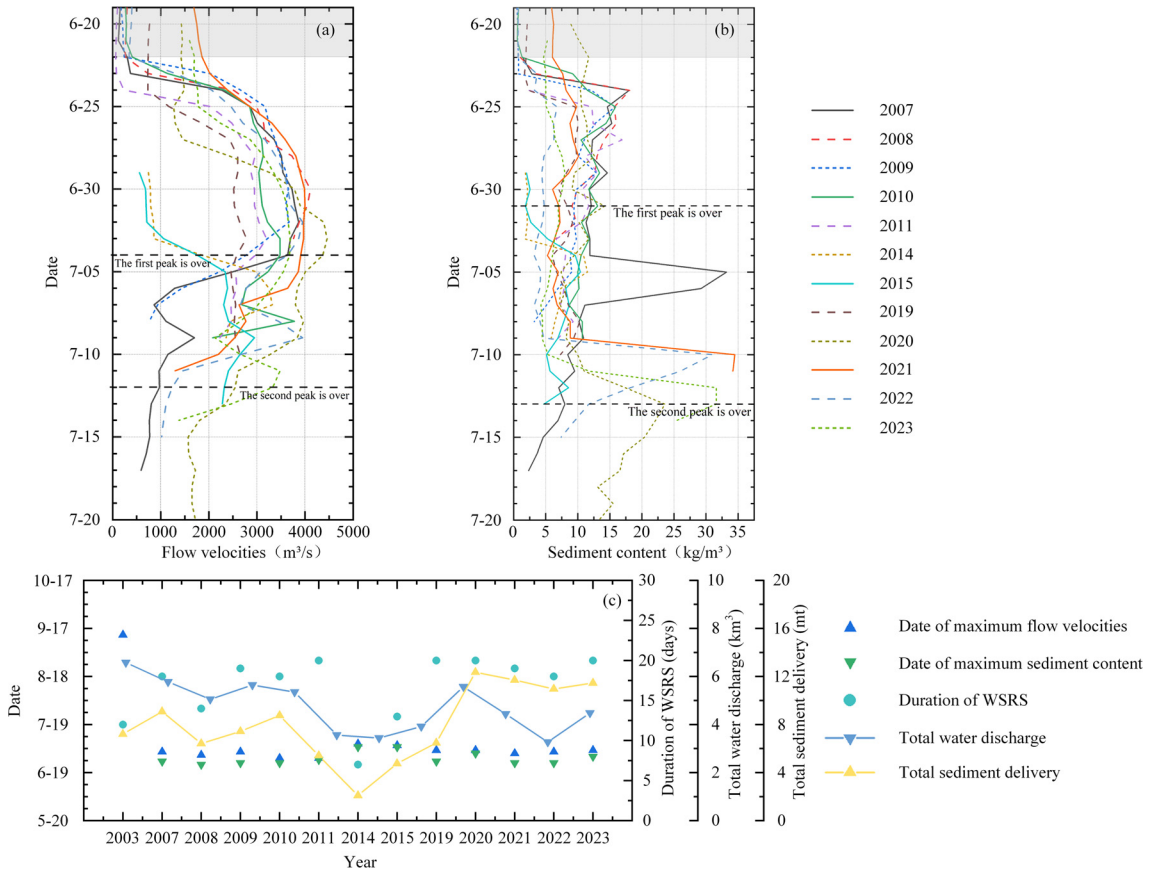

FIGURE 4
Annual analysis and compilation of data from WSRS events. **(a)** Daily runoff. **(b)** Daily sediment concentration. **(c)** Total water and sediment discharge, along with the annual operational duration during the WSRS period. WSRS, water–sediment regulation scheme.

4 Discussion

4.1 Response of plume patterns to river discharge

Among many forcings influencing the dispersion and dynamics of river plumes, river discharge has commonly been recognized as the primary driver dominating river plume dynamics (Salcedo-Castro et al., 2023; Fu et al., 2024). Focusing on the YRP, previous studies have documented that river discharge mainly determined the plume diffusion area and controlled the plume temporal variation on seasonal and daily scales (Wang et al., 2011; Cheng et al., 2021b). As illustrated in Figure 7, the significant correlation between the plume area and the total river discharge (R^2 = 0.45) indicated that upstream freshwater release also plays a major role in the significant interannual variations of the YRP. For instance, accompanied by a water discharge of 4.38 km^3, the river plume increased sharply to 150.39 km^2 in 2010. However, the relationship between plume area and river discharge revealed here was notably weaker than those derived from daily-scale data analysis (Guo et al., 2017). We speculate that this discrepancy may be attributed to external interannual forcing factors such as wind and tides (Wang et al., 2011; Jia and Yi, 2023). Furthermore, the method used to extract the plume boundary may align more closely with the suspended sediment boundary, potentially leading to an underestimation of the waterflow's effect on plum dispersion.

Focused on the significant interannual variations of the peak values and duration of the WSRS, no significant correlation was found between peak river discharge and plume area. In contrast, daily water discharge was significantly correlated with plume area (R^2 = 0.30). This finding suggested that, under the assumption of a constant total water discharge, impulsive delivery of water within a shorter duration may be more efficient in transporting plume waters further offshore.

4.2 Response of plume patterns to winds

Wind forcing is widely recognized as a critical factor influencing the plume structure and orientation (Chen et al., 2017). In summer, upwelling-favorable southerly and southeasterly winds prevail in the YRE; the northeastward Ekman transport pushed the low-saline water offshore, often extending to the central area of Bohai Sea in 2003, 2008, 2009, 2014, 2020, 2021, and 2022 (Figure 8). This phenomenon revealed using satellite data here was consistent with previous model results (Cheng et al., 2021b; Jia and Yi, 2023).

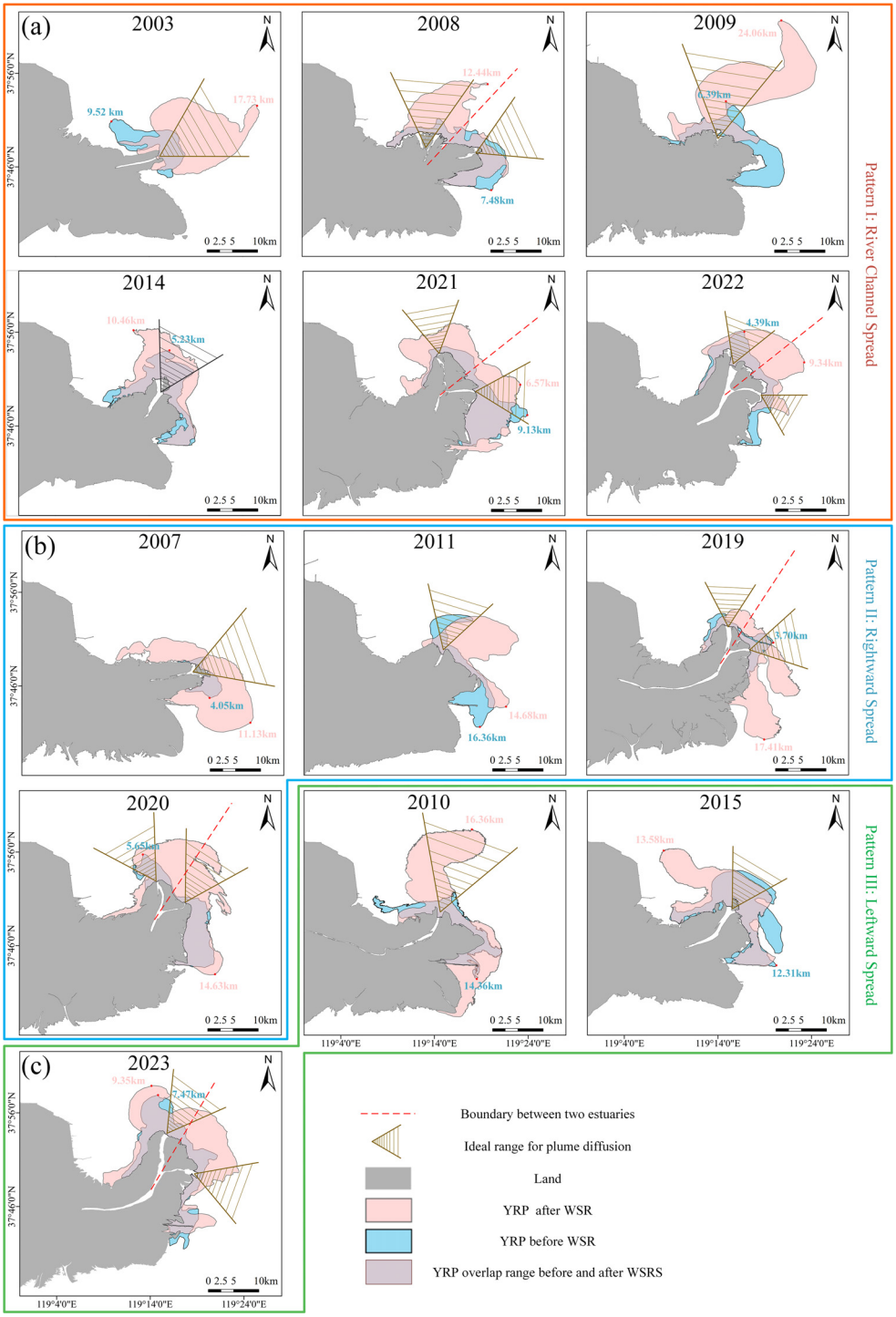

FIGURE 5
YRP before and after WSRS for each year. **(a)** Diffusion along the river channel. **(b)** Rightward shift diffusion. **(c)** Leftward shift diffusion. YRP, Yellow River turbid plume; WSRS, water–sediment regulation scheme.

However, in other years, including 2007, 2011, and 2019, when the wind was similarly southerly and southeasterly oriented, the estuarine plume moved southward into Laizhou Bay. This exceptional feature was also noted by Cheng et al. (2021b), with potential driving forces including the Coriolis, buoyancy, or tide currents (Yang et al., 2017; Cheng et al., 2021b; Jia and Yi, 2023). Occasionally, easterly wind fields occurred in 2015 and 2023, transporting plume water onshore along the west coast of the Bohai Sea.

In addition to wind directions, wind speed significantly impacted the plume's offshore spreading, similar to previous studies (Wang et al., 2008; Qin et al., 2023).

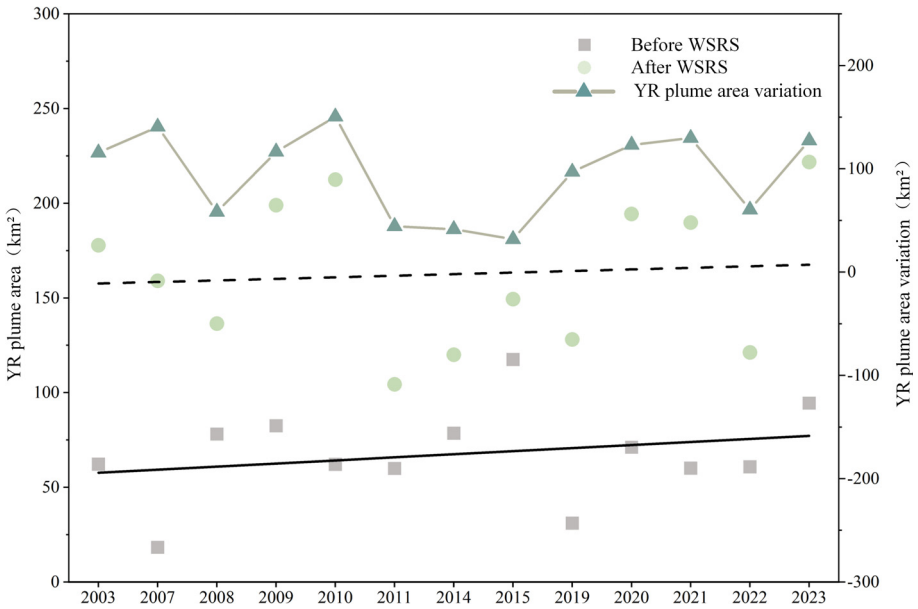

FIGURE 6
Analysis of YRP area variations before and after WSRS. YRP, Yellow River turbid plume; WSRS, water–sediment regulation scheme.

We observed that weak (<3.5 m/s) wind forcing favored plume offshore spreading, as seen in 2010, 2014, and 2015. On the contrary, strong (>5 m/s) winds tend to hinder the spreading of the YRP, thereby reducing its area. However, possibly due to the increased mixing and vertical extension of the plume water under high wind stress (Sandeep and Pant, 2019), no obvious relationship exists between wind speed and plume area.

To further clarify the favorable wind conditions for three YRP patterns, we used the wind rose plots to provide the overall view of the intensity and direction of the winds (Supplementary Figure S1). Plumes of Pattern I occur mostly under low (<6 m/s) southerly and southeasterly wind forcing, with the occurrence frequency exceeding 60%. Low (<8 m/s) and variable wind forcing usually result in Pattern II plumes. The favorable wind conditions for Pattern III are the easterly and southeasterly winds. However, years with special wind fields existed in any patterns of plumes: 2003 in Pattern I, 2011 in Pattern II, and 2023 in Pattern III. Winds in those years share similar characteristics: they were all strong (>10 m/s), in association with plume-oriented wind forcing. Thus, consistent with the study of Chen et al. (2017), we speculate that the strong wind forcing caused by episodic weather events may significantly affect the direction of the plume expansion.

Furthermore, based on the Finite Volume Coastal Ocean Model (FVCOM) three-dimensional model, Qin et al. (2023) demonstrated that intensifying winds drive a counterclockwise rotation of the YRP dispersion, shifting its trajectory from south to north. Our satellite observations align with this mechanistic understanding, as shown in Supplementary Figure S1, which revealed that wind speeds in the YRE were significantly higher during Pattern I plume events compared to Pattern II conditions. It should be noted that critical wind speed thresholds governing plume modality transitions may vary substantially across estuarine systems. Such thresholds remain to be quantified for estuaries with distinct geometric configurations and boundary conditions.

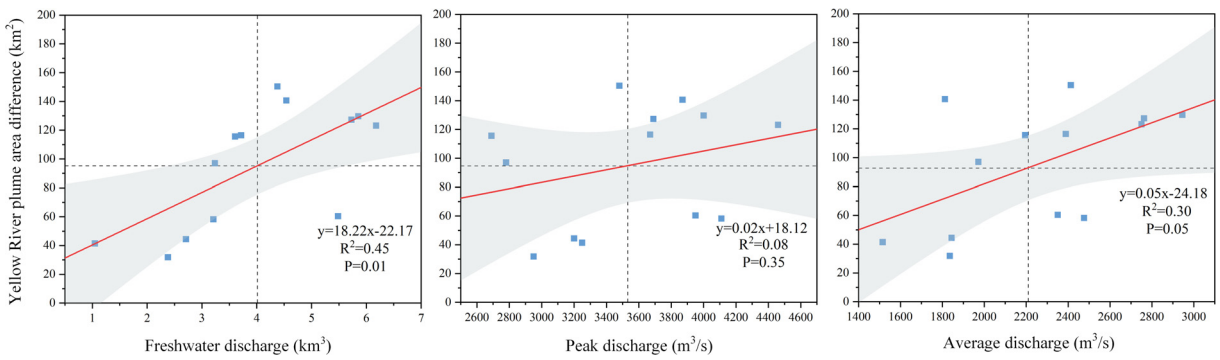

FIGURE 7
Correlation between the YRP flow and runoff during WSRS. YRP, Yellow River turbid plume; WSRS, water–sediment regulation scheme.

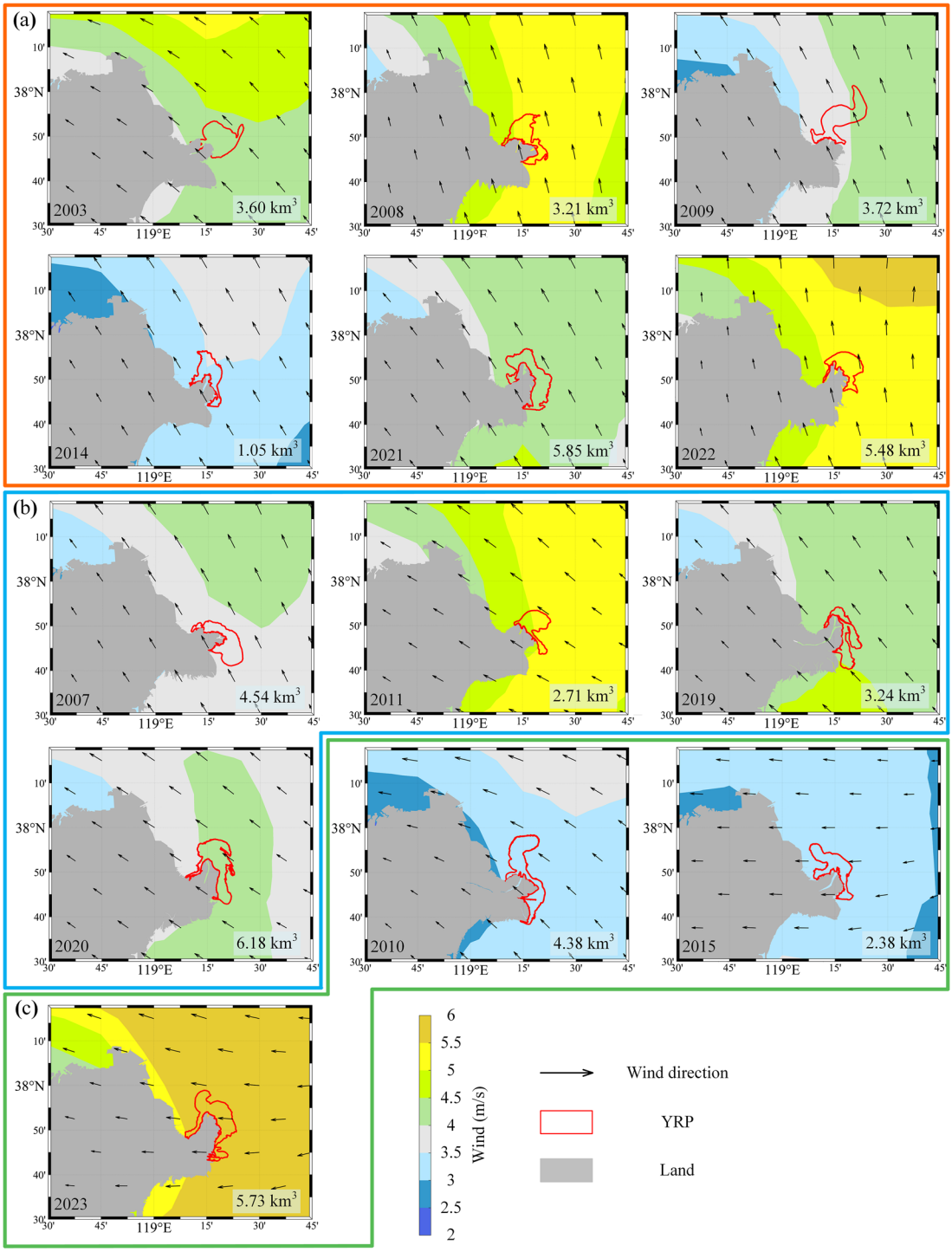

FIGURE 8
Mean wind fields during the WSRS and the corresponding Yellow River turbid plume (YRP) flow after the WSRS; the lower right corner is the freshwater discharge during WSRS period. WSRS, water–sediment regulation scheme. **(a)** Prototypical spreading plume. **(b)** Rightward spreading plume. **(c)** Leftward spreading plume.

4.3 Other influencing factors

In the previous sections, we mainly focused on the effect of river discharge and wind, which have commonly been recognized as the most important forcing mechanisms, on the dispersal of river plumes (Osadchiev et al., 2021; Machaieie et al., 2022; Salcedo-Castro et al., 2023). External forcing such as the geomorphology of river mouth (Lee and Valle-Levinson, 2013), coastal currents (Wang et al., 2008; Wang et al., 2010b; Ding et al., 2017; Xu et al., 2019), and waves (Jia and Yi, 2023) also influences the

spatial and temporal dispersion of river plumes in the ocean (Horner-Devine et al., 2015; Zhi et al., 2022).

The YRE experienced dramatic morphological evolution (Ji et al., 2018), which proved to be a key parameter in determining the structure and scale of river plumes (Lai et al., 2015; Cole and Hetland, 2016). As shown in Figure 5 and Supplementary Figure S2, in response to the dramatic evolution of the mouth channel and bar, before the WSRS, the plume fronts generally propagated offshore along the direction of channel expansion. This includes the eastward fan-shaped pattern observed in 2003, 2007, and 2008; the northeastward expansion structures from 2009 to 2015; and the bimodal structure (one extending toward the southeast and the

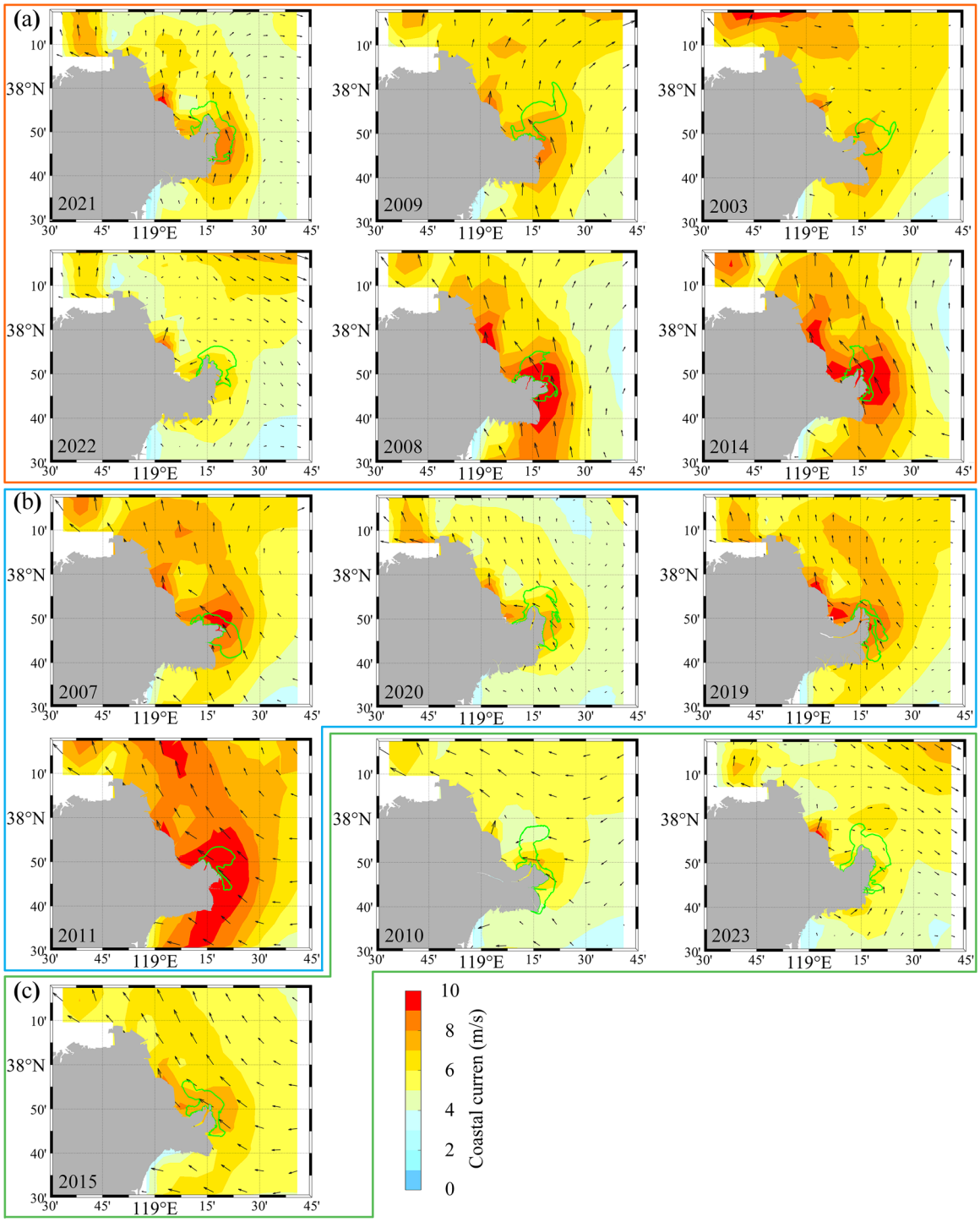

FIGURE 9
YRP after WSRS for each year. The plume flows are sorted by their area difference, from the largest difference to the smallest. **(a)** Diffusion along the river channel. **(b)** Rightward shift diffusion. **(c)** Leftward shift diffusion. YRP, Yellow River turbid plume; WSRS, water–sediment regulation scheme.

other toward the northeast) observed since 2019. The geometric shape of the mouth bar controlled the spatial extension of the turbid plume along the shoreline. Moreover, the plume spread more offshore in the northeastward channel. Lee and Valle-Levinson's (2013) work indicated that the direction of a submarine channel influenced plume characteristics with an ocean circulation model; the phenomenon observed confirmed this issue. However, after the WSRS, in addition to the Pattern I plume, the plume structures were no longer governed by estuarine morphology. Instead, the dispersion pattern of the plume was shown to be more complex and diverse, indicating the influence of estuarine morphology weakened under the impact of extreme freshwater discharge events.

Coastal currents are a significant forcing for nearshore sediment transport (Liu et al., 2020a; Li et al., 2021). The simulated current from the HYCOM showed that coastal circulation off the estuary generally flows northward and parallel to the coastline but exhibited significant interannual variations in current speed (Figure 9). In all years, except 2008, 2009, 2014, and 2015, the distribution of the river plume was mismatched with the current field. This implied that the impact of coastal currents on the long-term variation of river plumes has been minimal, similar to that described by Chang et al. (2022). In addition, for the Pattern II and Pattern III plumes, the offshore dispersion of the YRP was significantly inhibited when coastal currents were strong. However, our study was unable to clarify the impact of hyperpycnal flows, which are triggered by high sediment concentrations and have been documented to significantly influence sediment dispersal patterns (Wang et al., 2010a; Wu et al., 2023) on the spatio-temporal variations of the river plume. Further in-depth research is needed to address this aspect in the future.

Waves and tides also are the two important ones affecting the transport of water and sediment, thus influencing the dispersion of river plumes (Cheng et al., 2023; Du et al., 2023). The roles they play in the interannual variation of river plumes under WSRS scenarios need further studies.

5 Conclusions

Multi-source high-resolution satellite imageries were analyzed to characterize the structure and variability of the YRP, particularly under the influence of the WSRS implemented since 2002. The WSRS-induced pulse discharge of freshwater and sediment led to a sharp increase in plume area and formed three distinct plume patterns, including I) prototypical spreading along the river channel, II) rightward spreading toward Laizhou Bay, and III) leftward spreading toward Bohai Bay.

River discharge and wind forcing were identified as the dominant external factors modulating YRP dynamics. River discharge emerged as the primary control on plume size, with pulsed water delivery during shorter WSRS durations proving particularly effective in enhancing freshwater offshore transport. Wind exerted critical control over plume directionality: consistent southerly/southeasterly winds favored Pattern I's along-channel dispersion, while easterly/southeasterly winds drove Pattern III's leftward deflection into Bohai Bay. Pattern II's rightward expansion into Laizhou Bay occurred under more variable wind conditions. Notably, episodic weather events generating strong winds were found to abruptly alter plume trajectories, demonstrating the system's heightened sensitivity to extreme meteorological forcing.

These findings highlight the complex interplay between natural processes and human interventions in shaping plume dynamics, demonstrating how the WSRS has become a dominant control mechanism alongside natural forcings. While this study significantly advances our comprehension of interannual plume variability in the Yellow River system, two critical knowledge gaps persist: 1) the complex wave–tide interactions and their synergistic effects on sediment dispersal patterns during WSRS events and 2) the daily-scale plume responses to short-term meteorological forcing and anthropogenic perturbations. These unresolved questions particularly limit our ability to predict high-frequency plume dynamics during extreme discharge pulses, highlighting the need for targeted investigations combining high-resolution monitoring with numerical simulations.

Data availability statement

The original contributions presented in the study are included in the article/Supplementary Material. Further inquiries can be directed to the corresponding authors.

Author contributions

FW: Data curation, Formal Analysis, Investigation, Validation, Writing – original draft. XB: Conceptualization, Methodology, Supervision, Validation, Writing – review & editing. FQ: Conceptualization, Funding acquisition, Methodology, Validation, Writing – original draft, Writing – review & editing. TZ: Formal Analysis, Investigation, Project administration, Supervision, Writing – review & editing. XW: Data curation, Methodology, Validation, Writing – review & editing. LM: Conceptualization, Funding acquisition, Methodology, Software, Validation, Writing – original draft, Writing – review & editing.

Funding

The author(s) declare that financial support was received for the research and/or publication of this article. L. Meng obtained funding from the National Natural Science Foundation of China (Grant No. 42406193) independently. L. Meng and F. Qu received Natural Science Foundation of Shandong Province grants (Grant Nos. ZR2020QD092 and ZR2023MD046, respectively).

Conflict of interest

The authors declare that the research was conducted in the absence of any commercial or financial relationships that could be construed as a potential conflict of interest.

The reviewer DS declared a past co-authorship with the author FQ to the handling editor.

Generative AI statement

The author(s) declare that no Generative AI was used in the creation of this manuscript.

Publisher's note

Supplementary material

The Supplementary Material for this article can be found online at: https://www.frontiersin.org/articles/10.3389/fmars.2025.1535411/full#supplementary-material

References

Aurin, D., Mannino, A., and Franz, B. (2013). Spatially resolving ocean color and sediment dispersion in river plumes, coastal systems, and continental shelf waters. *Remote Sens. Environ.* 137, 212–225. doi: 10.1016/j.rse.2013.06.018

Bi, N., Yang, Z., Wang, H., Hu, B., and Ji, Y. (2010). Sediment dispersion pattern off the present Huanghe (Yellow River) subdelta and its dynamic mechanism during normal river discharge period. *Estuarine Coastal Shelf Sci.* 86, 352–362. doi: 10.1016/j.ecss.2009.06.005

Binding, C. E., and Bowers, D. G. (2003). Measuring the salinity of the Clyde Sea from remotely sensed ocean colour. *Estuarine Coastal Shelf Sci.* 57, 605–611. doi: 10.1016/S0272-7714(02)00399-2

Cai, Z., Zhang, Z., Zhao, F., Guo, X., Zhao, J., Xu, Y., et al. (2023). Assessment of eco-environmental quality changes and spatial heterogeneity in the Yellow River Delta based on the remote sensing ecological index and geo-detector model. *Ecol. Inform.* 77, 102203. doi: 10.1016/j.ecoinf.2023.102203

Chang, M., Li, P., Sun, Y., Wang, H., and Li, Z. (2022). Mapping dynamic turbidity maximum zone of the yellow river estuary from 38 years of landsat imagery. *Remote Sens.* 14, 3782. doi: 10.3390/rs14153782

Chen, Z., Gong, W., Cai, H., Chen, Y., and Zhang, H. (2017). Dispersal of the Pearl River plume over continental shelf in summer. *Estuarine Estuar. Coast. Shelf Sci.* 194, 252–262. doi: 10.1016/j.ecss.2017.06.025

Cheng, X., Zhu, J., and Chen, S. (2021a). Dynamics of the extension of the Yellow River plume in the Bohai Sea. *Cont. Shelf Res.* 222, 104438. doi: 10.1016/j.csr.2021.104438

Cheng, X., Zhu, J., and Chen, S. (2021b). Extensions of the river plume under various Yellow River courses into the Bohai Sea at different times. *Estuar. Coastal Shelf Sci.* 249, 107092. doi: 10.1016/j.ecss.2020.107092

Cheng, X., Zhu, J., and Chen, S. (2023). Dynamic response of water flow and sediment transport off the Yellow River mouth to tides and waves in winter. *Front. Mar. Sci.* 10. doi: 10.3389/fmars.2023.1181347

Chu, Z., Sun, X., Zhai, S., and Xu, K. (2006). Changing pattern of accretion/erosion of the modern Yellow River Huanghe subaerial delta, China: Based on remote sensing images. *Mar. Geol.* 227, 13–30. doi: 10.1016/j.margeo.2005.11.013

Cole, K. L., and Hetland, R. D. (2016). The effects of rotation and river discharge on net mixing in small-mouth kelvin number plumes. *J. Phys. Oceanogr.* 46, 1421–1436. doi: 10.1175/JPO-D-13-0271.1

Ding, Y., Bao, X., Yao, Z., Zhang, C., Wan, K., Bao, M., et al. (2017). A modeling study of the characteristics and mechanism of the westward coastal current during summer in the northwestern South China Sea. *Ocean Sci. J.* 52, 11–30. doi: 10.1007/s12601-017-0011-x

Du, Y., Zhang, J., Bian, C., Fang, X., Cheng, J., Wang, G., et al. (2023). Multiscale spatio-temporal variations of suspended sediment fronts in the semi-enclosed Bohai Sea, China. *J. Geophys. Res. Oceans* 128, 11. doi: 10.1029/2023JC019773

Fernández-Nóvoa, D., Mendes, R., deCastro, M., Dias, J. M., Sánchez-Arcilla, A., and Gómez-Gesteira, M. (2015). Analysis of the influence of river discharge and wind on the Ebro turbid plume using MODIS-Aqua and MODIS-Terra data. *J. Mar. Syst.* 142, 40–46. doi: 10.1016/j.jmarsys.2014.09.009

Fu, Y., Chen, S., Ji, H., Fan, Y., and Li, P. (2021). The modern Yellow River Delta in transition: Causes and implications. *Mar. Geol.* 436, 106476. doi: 10.1016/j.margeo.2021.106476

Fu, Y., Wang, Z., Zhao, M., Song, X., Jia, Y., and Song, Z. (2024). Factors influencing the variation of the Sepik-Ramu River system's sediment plume off the north coast of New Guinea. *Estuar. Coastal Shelf Sci.* 303, 108782. doi: 10.1016/j.ecss.2024.108782

Guo, K., Zou, T., Jiang, D., Tang, C., and Zhang, H. (2017). Variability of Yellow River turbid plume detected with satellite remote sensing during water-sediment regulation. *Cont. Shelf Res.* 135, 74–85. doi: 10.1016/j.csr.2017.01.017

Horner-Devine, A. R., Hetland, R. D., and MacDonald, D. G. (2015). Mixing and transport in coastal river plumes. *Annu. Rev. Fluid Mech.* 47, 569–594. doi: 10.1146/annurev-fluid-010313-141408

Ji, H., Chen, S., Pan, S., Xu, C., Jiang, C., and Fan, Y. (2018). Morphological variability of the active Yellow River mouth under the new regime of riverine delivery. *J. Hydrol.* 564, 329–341. doi: 10.1016/j.jhydrol.2018.07.014

Jia, W., and Yi, Y. (2023). Numerical study of the water-sediment regulation scheme WSRS impact on suspended sediment transport in the Yellow River Estuary. *Front. Mar. Sci.* 10. doi: 10.3389/fmars.2023.1135118

Lai, Z., Ma, R., Gao, G., Chen, C., and Beardsley, R. (2015). Impact of multichannel river network on the plume dynamics in the Pearl River estuary. *J. Geophys. Res. Oceans.* 20, 5766–5789. doi: 10.1002/2014jc010490

Lee, J., and Valle-Levinson, A. (2013). Bathymetric effects on estuarine plume dynamics. *J. Geophys. Res. Oceans.* 118, 1969–1981. doi: 10.1002/jgrc.20119

Li, P., Chen, S., Ji, H., Fan, Y., Fu, Y., Ran, B., et al. (2023). Detecting the magical yellow-blue demarcation off the Yellow River Estuary from the space. *Front. Mar. Sci.* 10. doi: 10.3389/fmars.2023.1234631

Li, P., Chen, S., Ji, H., Ke, Y., and Fu, Y. (2021). Combining Landsat-8 and Sentinel-2 to investigate seasonal changes of suspended particulate matter off the abandoned distributary mouths of Yellow River Delta. *Mar. Geol.* 441, 106622. doi: 10.1016/j.margeo.2021.106622

Li, X., Chen, H., Jiang, X., Yu, Z., and Yao, Q. (2017). Impacts of human activities on nutrient transport in the Yellow River: The role of the Water-Sediment Regulation Scheme. *Sci. Total Environ.* 592, 161–170. doi: 10.1016/j.scitotenv.2017.03.098

Liu, X., Qiao, L., Zhong, Y., Wan, X., Xue, W., and Liu, P. (2020a). Pathways of suspended sediments transported from the Yellow River mouth to the Bohai Sea and Yellow Sea. *Estuar. Coast. Shelf Sci.* 236, 106639. doi: 10.1016/j.ecss.2020.106639

Liu, Z., Xu, N., and Wang, J. (2020b). Satellite-observed evolution dynamics of the Yellow River Delta in 1984–2018. *IEEE J. Sel. Top. Appl. Earth Obs. Remote Sens.* 13, 6044–6050. doi: 10.1109/jstars.2020.3026708

Lu, T., Wang, H., Wu, X., Bi, N., Hu, L., and Bianchi, T. S. (2022). Transport of particulate organic carbon in the lower Yellow River Huanghe as modulated by dam operation. *Glob. Planet. Change* 217, 103948. doi: 10.1016/j.gloplacha.2022.103948

Lv, X., Yuan, D., Ma, X., and Tao, J. (2014). Wave characteristics analysis in Bohai Sea based on ECMWF wind field. *Ocean Eng.* 91, 159–171. doi: 10.1016/j.oceaneng.2014.09.010

Machaieie, H., Nehama, F., Silva, C., and Negri, E. (2022). Satellite assessment of coastal plume variability and its relation to environmental variables in the Sofala Bank. *Front. Mar. Sci.* 9. doi: 10.3389/fmars.2022.897429

Maciel, F. P., Santoro, P. E., and Pedocchi, F. (2021). Spatio-temporal dynamics of the Río de la Plata turbidity front; combining remote sensing with *in-situ* measurements and numerical modeling. *Cont. Shelf Res.* 213, 104301. doi: 10.1016/j.csr.2020.104301

Mendes, R., Saldías, G. S., deCastro, M., Gómez-Gesteira, M., Vaz, N., and Dias, J. M. (2017). Seasonal and interannual variability of the Douro turbid river plume, northwestern Iberian Peninsula. *Remote Sens. Environ.* 194, 401–411. doi: 10.1016/j.rse.2017.04.001

Molleri, G. S. F., Novo, E., and Kampel, M. (2010). Space-time variability of the Amazon River plume based on satellite ocean color. *Cont. Shelf Res.* 30, 342–352. doi: 10.1016/j.csr.2009.11.015

Osadchiev, A., Sedakov, R., and Barymova, A. (2021). Response of a small river plume on wind forcing. *Front. Mar. Sci.* 8. doi: 10.3389/fmars.2021.809566

Peng, J., Chen, S., and Dong, P. (2010). Temporal variation of sediment load in the Yellow River basin, China, and its impacts on the lower reaches and the river delta. *Catena* 83, 135–147. doi: 10.1016/j.catena.2010.08.006

Qin, H., Shi, H., Gai, Y., Qiao, S., and Li, Q. (2023). Sensitivity analysis of runoff and wind with respect to yellow river estuary salinity plume based on FVCOM. *Water* 15, 1378. doi: 10.3390/w15071378

Salcedo-Castro, J., Olita, A., Saavedra, F., Saldías, G. S., Cruz-Gómez, R. C., and de la Torre Martínez, C. D. (2023). Modeling the interannual variability in Maipo and Rapel river plumes off central Chile. *Ocean Sci.* 19, 1687–1703. doi: 10.5194/os-19-1687-2023

Sandeep, K. K., and Pant, V. (2019). Riverine freshwater plume variability in the Bay of Bengal using wind sensitivity experiments. *Deep Sea Res. Part II Top. Stud. Oceanogr.* 168, 104649. doi: 10.1016/j.dsr2.2019.104649

Wang, H., Bi, N., Saito, Y., Wang, Y., Sun, X., Zhang, J., et al. (2010a). Recent changes in sediment delivery by the Huanghe Yellow River to the sea: Causes and environmental implications in its estuary. *J. Hydrol.* 391, 302–313. doi: 10.1016/j.jhydrol.2010.07.030

Wang, H., Bi, N., Wang, Y., Saito, Y., and Yang, Z. (2010b). Tide-modulated hyperpycnal flows off the Huanghe (Yellow River) mouth, China. *Earth Surf. Proc. Land.* 35, 1315–1329. doi: 10.1002/esp.2032

Wang, S., Fu, B., Liang, W., Liu, Y., and Wang, Y. (2017b). Driving forces of changes in the water and sediment relationship in the Yellow River. *Sci. Total Environ.* 576, 453–461. doi: 10.1016/j.scitotenv.2016.10.124

Wang, Q., Guo, X., and Takeoka, H. (2008). Seasonal variations of the Yellow River plume in the Bohai Sea: A model study. *J. Geophys. Res.* 113, C08046. doi: 10.1029/2007jc004555

Wang, Y., Liu, Z., Gao, H., Ju, L., and Guo, X. (2011). Response of salinity distribution around the Yellow River mouth to abrupt changes in river discharge. *Cont. Shelf Res.* 31, 685–694. doi: 10.1016/j.csr.2011.01.005

Wang, Y., Liu, D., Lee, K., Dong, Z., Di, B., Wang, Y., et al. (2017c). Impact of Water-Sediment Regulation Scheme on seasonal and spatial variations of biogeochemical factors in the Yellow River estuary. *Estuar. Coast. Shelf Sci.* 198, 92–105. doi: 10.1016/j.ecss.2017.09.005

Wang, A., Wang, H., Bi, N., and Wu, X. (2016). Sediment transport and dispersal pattern from the Bohai Sea to the Yellow Sea. *J. Coastal Res.* 74, 104–116. doi: 10.2112/si74–010.1

Wang, H., Wang, A., Bi, N., Zeng, X., and Xiao, H. (2014). Seasonal distribution of suspended sediment in the Bohai Sea, China. *Cont. Shelf Res.* 90, 17–32. doi: 10.1016/j.csr.2014.03.006

Wang, H., Wu, X., Bi, N., Li, S., Yuan, P., Wang, A., et al. (2017a). Impacts of the dam-orientated water-sediment regulation scheme on the lower reaches and delta of the Yellow River Huanghe: A review. *Glob. Planet. Change* 157, 93–113. doi: 10.1016/j.gloplacha.2017.08.005

Wang, H., Yang, Z., Bi, N., and Li, H. (2005). Rapid shifts of the river plume pathway off the Huanghe (Yellow) River mouth in response to water-sediment regulation scheme in 2005. *Chin. Sci. Bull.* 50, 2878–2884. doi: 10.1360/982005-1196

Warrick, J. A., and Farnsworth, K. L. (2017). Coastal river plumes: Collisions and coalescence. *Prog. Oceanogr.* 151, 245–260. doi: 10.1016/j.pocean.2016.11.008

Wu, G., Wang, K., Liang, B., Wu, X., Wang, H., Li, H., et al. (2023). Modeling the morphological responses of the Yellow River Delta to the water-sediment regulation scheme: The role of impulsive river floods and density-driven flows. *Water Resour. Res.* 59, e2022WR033003. doi: 10.1029/2022WR033003

Xu, C., Xu, Y., Hu, J., Li, S., and Wang, B. (2019). A numerical analysis of the summertime Pearl River plume from 1999 to 2010: Dispersal patterns and intraseasonal variability. *J. Mar. Syst.* 192, 15–27. doi: 10.1016/j.jmarsys.2018.12.010

Yan, C. (2019). The variation and influencing factors of the runoff and sediment entering sea in the Yellow River. *IOP Conf. Ser. Earth Environ. Sci.* 330, 32057. doi: 10.1088/1755-1315/330/3/032057

Yang, H., Li, E., Zhao, Y., and Liang, Q. (2017). Effect of water-sediment regulation and its impact on coastline and suspended sediment concentration in Yellow River Estuary. *Water Sci. Eng.* 10, 311–319. doi: 10.1016/j.wse.2017.12.009

Yu, X., Guo, X., Gao, H., and Zou, T. (2021). Upstream extension of a bottom-advected plume and its mechanism: the case of the yellow river. *J. Phys. Oceanogr.* 51, 2351–2371. doi: 10.1175/JPO-D-20-0235.1

Yu, Y., Shi, X., Chi, W., Hu, Z., and Qiao, S. (2013a). Hourly change in sediment plume at Yellow River mouth during the water-sediment regulation. *Mar. Geol. Quat. Geol.* 38, 41–51. doi: 10.16562/j.cnki.0256-1492.2018.05.004

Yu, Y., Shi, X., Wang, H., Yue, C., Chen, S., Liu, Y., et al. (2013b). Effects of dams on water and sediment delivery to the sea by the Huanghe (Yellow River): The special role of Water-Sediment Modulation. *Anthropocene* 3, 72–82. doi: 10.1016/j.ancene.2014.03.001

Yu, X., Guo, X., Gao, H., and Zou, T. (2021). Upstream extension of a bottom-advected plume and its mechanism: the case of the yellow river. *J. Phys. Oceanogr.* 51, 2351–2371. doi: 10.1175/JPO-D-20-0235.1

Yuan, D., Du, M., Yan, C., Wang, J., Wang, C., Zhu, Y., et al. (2024). Coupling coordination degree analysis and spatiotemporal heterogeneity between water ecosystem service value and water system in Yellow River Basin cities. *Ecol. Inform.* 79, 102440. doi: 10.1016/j.ecoinf.2023.102440

Zhao, S., Yang, Z., Zhang, S., Wu, J., Zhao, Z., Jeng, D.-S., et al. (2023). Predictions of runoff and sediment discharge at the lower Yellow River Delta using basin irrigation data. *Ecol. Inform.* 78, 102385. doi: 10.1016/j.ecoinf.2023.102385

Zhi, H., Wu, H., Wu, J., Zhang, W., and Wang, Y. (2022). River plume rooted on the sea-floor: seasonal and spring-neap variability of the Pearl River plume. *Front. Mar. Sci.* 9. doi: 10.3389/fmars.2022.791948